Photo-CIDNP MAS NMR in Intact Cells of *Rhodobacter sphaeroides* R26: Molecular and Atomic Resolution at Nanomolar Concentration

Shipra Prakash,[†] Alia,[†] Peter Gast,[‡] Huub J. M. de Groot,[†] Jörg Matysik,*,[†] and Gunnar Jeschke[§]

Contributions from the Leiden Institute of Chemistry, P.O. Box 9502, 2300 RA Leiden, The Netherlands, Leiden Institute of Physics, P.O. Box 9504, 2300 RA Leiden, The Netherlands, and Department of Chemistry, University of Konstanz, 78457 Konstanz, Germany

Received April 6, 2006; E-mail: j.matysik@chem.leidenuniv.nl

Abstract: Photochemically induced dynamic nuclear polarization (photo-CIDNP) is observed in photosynthetic reaction centers of the carotenoid-less strain R26 of the purple bacterium *Rhodobacter sphaeroides* by ^{13}C solid-state NMR at three different magnetic fields (4.7, 9.4, and 17.6 T). The signals of the donor appear enhanced absorptive (positive) and of the acceptor emissive (negative). This spectral feature is in contrast to photo-CIDNP data of reactions centers of *Rhodobacter sphaeroides* wildtype reported previously (Prakash, S.; Alia; Gast, P.; de Groot, H. J. M.; Jeschke, G.; Matysik, J. *J. Am. Chem. Soc.* **2005**, *127*, 14290−14298) in which all signals appear emissive. The difference is due to an additional mechanism occurring in RCs of R26 in the long-living triplet state of the donor, allowing for spectral editing by different enhancement mechanisms. The overall shape of the spectra remains independent of the magnetic field. The strongest enhancement is observed at 4.7 T, enabling the observation of photo-CIDNP enhanced NMR signals from reaction center cofactors in entire bacterial cells allowing for detection of subtle changes in the electronic structure at nanomolar concentration of the donor cofactor. Therefore, we establish in this paper photo-CIDNP MAS NMR as a method to study the electronic structure of photosynthetic cofactors at the molecular and atomic resolution as well as at cellular concentrations.

Introduction

Photochemically induced dynamic nuclear polarization (photo-CIDNP) is a method to increase NMR intensities by induction of photochemical reactions, which shuffle the nuclear spin system out of its Boltzmann equilibrium. In contrast to optical pumping, photo-CIDNP does not require polarized radiation. Photo-CIDNP in solution NMR[1,2] is explained by the radical-pair mechanism where a certain nucleus of a reactant gains opposite polarization in cage products created via a singlet pathway and escape products created via a triplet pathway. Because of the different chemical nature of the cage and escape products and thus the different chemical shift of the nucleus in the products, these polarizations can be observed separately.[3,4] This mechanism is not observable for a cyclic reaction where the opposite polarization cancels and is hardly feasible in the solid state at all for lack of diffusion that could lead to product branching depending on the spin state of the spin-correlated radical pair. In solids, photo-CIDNP can be observed by magic-angle spinning (MAS) NMR, a method which overcomes line-broadening due to chemical shift anisotropy (CSA) in solids and allows for detailed analysis of structure, dynamics, and functional mechanisms of membrane-bound protein systems.[5,6] In the solid state, photo-CIDNP has been observed for the first time in quinone blocked frozen reaction centres (RCs) of *Rhodobacter (Rb.) sphaeroides* R26[7−10] and WT[11−13] under continuous illumination with white light (for review on bacterial RCs, see ref 14). Photo-CIDNP has been observed not only in bacterial RCs but in plant photosystems I[15] and II[16,17] as well.

[†] Leiden Institute of Chemistry.
[‡] Leiden Institute of Physics.
[§] University of Konstanz.
(1) Hore, P. J.; Broadhurst, R. W. *Prog. Nucl. Magn. Reson. Spectrosc.* **1993**, *25*, 345−402.
(2) Goez, M. *Adv. Photochem.* **1997**, *23*, 63−164.
(3) Closs, G. L.; Closs, L. E. *J. Am. Chem. Soc.* **1969**, *91*, 4549−4550.
(4) Kaptein, R.; Oosterhoff, J. L. *Chem. Phys. Lett.* **1969**, *4*, 195−197.

(5) de Groot, H. J. M. *Curr. Opin. Struct. Biol.* **2000**, *10*, 593−600.
(6) Laws, D. D.; Bitter, H. M. L.; Jerschow, A. *Angew. Chem., Int. Ed.* **2002**, *41*, 3096−3129.
(7) Zysmilich, M. G.; McDermott, A. *J. Am. Chem. Soc.* **1994**, *116*, 8362−8363.
(8) Zysmilich, M. G.; McDermott, A. *J. Am. Chem. Soc.* **1996**, *118*, 5867−5873.
(9) Zysmilich, M. G.; McDermott, A. *Proc. Natl. Acad. Sci. U.S.A.* **1996**, *93*, 6857−6860.
(10) Matysik, J.; Alia; Hollander, J. G.; Egorova-Zachernyuk, T.; Gast, P.; de Groot, H. J. M. *Indian J. Biochem. Biophys.* **2000**, *37*, 418−423.
(11) Matysik, J.; Alia; Gast, P.; Lugtenburg, J.; Hoff, A. J.; de Groot, H. J. M. In *Perspectives on Solid State NMR in Biology;* Kiihne, S., de Groot, H. J. M., Eds.; Kluwer: Dordrecht, The Netherlands, 2001; p 215−225.
(12) Schulten, E. A. M.; Matysik, J.; Alia; Kiihne, S.; Raap, J.; Lugtenburg, J.; Gast, P.; Hoff, A. J.; de Groot, H. J. M. *Biochemistry* **2002**, *41*, 8708−8717.
(13) Prakash, S.; Alia; Gast, P.; de Groot, H. J. M.; Jeschke, G.; Matysik, J. *J. Am. Chem. Soc.* **2005**, *127*, 14290−14298.
(14) Hoff, A. J.; Deisenhofer, J. *Phys. Rep.* **1997**, *287*, 2−247.
(15) Alia; Roy, E.; Gast, P.; van Gorkom, H. J.; de Groot, H. J. M.; Jeschke, G.; Matysik, J. *J. Am. Chem. Soc.* **2004**, *126*, 12819−12826.
(16) Matysik, J.; Alia; Gast, P.; van Gorkom, H. J.; Hoff, A. J.; de Groot, H. J. M. *Proc. Natl. Acad. Sci. U.S.A.* **2000**, *97*, 9865−9870.
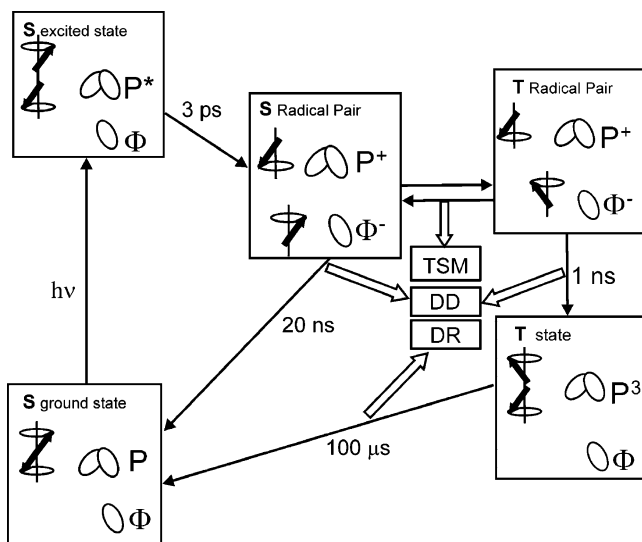
Figure 1. Reaction cycle in quinone blocked bacterial RCs. After light-induced electron transfer from the primary donor (P) to the bacteriopheophytin (ϕ), an electron polarized singlet radical pair is formed. The electron polarization is transferred to nuclei via three-spin mixing (TSM) within the radical pair and via differential decay (DD) owing to the difference in lifetime of the two radical pair states. Cancellation of incomplete nuclear spin polarization during long-lived donor triplet is by differential relaxation (DR). Kinetic data are taken from refs 14 and 21.

Upon photochemical excitation of the primary electron donor P, which is in RCs of purple bacteria, a BChl dimer composed of P_L and P_M, an electron is transferred to the primary acceptor, a bacteriopheophytin (BPhe) molecule ϕ, forming an electron-polarized singlet radical pair (Figure 1). In quinone reduced or depleted RCs, further electron transfer is blocked. Therefore, the singlet radical pair can either undergo back electron transfer to the electronic ground-state or, depending on the strength of the applied magnetic field, is transferred to a triplet radical pair. The triplet radical pair recombines to a special pair triplet ^3P and an acceptor singlet. Finally, the donor triplet is converted by radiationless decay to the singlet ground-state, so that the entire process is cyclic and opposite polarization originating from singlet and triplet spin-correlated radical pairs cancels.

If the nuclear spin relaxation is significant during the lifetime of the triplet state, this cancellation is not complete.[18] Such differential relaxation (DR) was predicted for photosynthetic RCs[19] and later invoked for explanation of the first experimental solid-state photo-CIDNP results.[20] However, the DR mechanism could not explain the observed signals from the bacteriopheophytin acceptor, which does not undergo intersystem crossing, and from wild-type RCs with a triplet lifetime that is by 3 orders of magnitude shorter. Photo-CIDNP in solids has thus been explained by the simultaneous action of two other mechanisms.[21] In the electron–electron–nuclear three-spin mixing (TSM) mechanism, net nuclear polarization is created in the spin-correlated radical pair owing to the presence of both anisotropic hyperfine interaction and coupling between the two electron

spins.[22] In the differential decay (DD) mechanism, a net photo-CIDNP effect is caused by anisotropic hyperfine coupling without an explicit requirement for electron–electron coupling if spin-correlated radical pairs have different lifetimes in their singlet and triplet states.[23]

On the basis of this approach of two parallel mechanisms, very recently we have been able to explain quantitatively the ^{13}C photo-CIDNP spectrum of WT RCs,[13] which shows entirely emissive photo-CIDNP signals. However, in RCs of the carotenoidless R26 strain, having a long lifetime of the donor triplet, the donor signals appear enhanced absorptive. This raises the question whether the DR mechanism is operative in the carotenoidless strain in addition to the two other mechanisms. The present contribution examines this question and on the basis of the understanding of the origin of the polarization patterns discusses subtle differences in the electronic structure of the radical pair between RCs of the WT and R26 strains as well as between isolated RCs and whole cells of the R26 strain.

Materials and Methods

Sample Preparation. The reaction centers (RCs) from *Rb. sphaeroides* R26 were isolated by the procedure of Feher and Okamura.[24] The removal of Q_A has been done by incubating the RCs at a concentration of 0.6 μM in 4% LDAO, 10 mM *o*-phenanthroline, 10 mM Tris buffer, pH 8.0, for 6 h at 26 °C, followed by washing with 0.5 M NaCl in 10 mM Tris buffer, pH 8.0, containing 0.025% LDAO and 1mM EDTA.[25] Approximately 5 mg of the RC protein complex embedded in LDAO micelles was used for NMR measurements.

The cells were harvested and suspended in Tris buffer. A total of 70 μL of this cell suspension was used for the experiment. The RCs in the cells were reduced with 0.05 M sodium dithionite in Tris buffer prior to experiments.

MAS-NMR Measurements. The NMR experiments at different fields were performed with DSX-750, DMX-400, and DMX-200 NMR spectrometers equipped with MAS probe (Bruker, Karlsruhe, Germany). The sample was loaded into a clear 4-mm sapphire rotor and inserted into the MAS probe. The sample was frozen slowly at a low spinning frequency of $\nu_r = 400$ Hz to ensure a homogeneous sample distribution against the rotor wall.[26] The light and dark spectra were collected with a Hahn echo pulse sequence and TPPM proton decoupling.[27] ^{13}C MAS NMR spectra were obtained at a temperature of 223 K under continuous illumination with white light.[10]

The rotational frequency for MAS was 8 kHz in all the experiments. For the three fields of 4.7, 9.6, and 17.6 T, a line broadening of 20, 50, and 120 Hz, respectively, was applied prior to Fourier transformation. In all cases, a cycle delay of 4 s was used. All the ^{13}C MAS NMR spectra were referenced to the $^{13}COOH$ response of solid tyrosine·HCl at 172.1 ppm.

Concentration of Special Pair Bacteriochlorophyll (BChl) Molecules. Optical density of the sample at 865 nm has been determined to be 1.28. Using an absorption coefficient of 75 mM^{-1}cm^{-1} and a typical ratio of special pair BChls to all BChl *a* cofactors of 2:300,[28] a sample concentration of ∼100 nM has been calculated.

(17) Diller, A.; Alia; Roy, E.; Gast, P.; van Gorkom, H. J.; de Groot, H. J. M.; Zaanen, J.; Glaubitz, C.; Matysik, J. *Photosynth. Res.* **2005**, *84*, 303−304.
(18) Hore, P. J.; Kaptein, R. In *NMR spectroscopy: New Methods and Applications*; Levy, G. C., Ed.; ACS Symposium 191; American Chemical Society: Washington, DC, 1982; p 285−318.
(19) Goldstein, R. A.; Boxer, S. G. *Biophys. J.* **1987**, *51*, 937−946.
(20) McDermott, A.; Zysmilich, M. G.; Polenova, T. *Solid State Magn. Reson.* **1998**, *11*, 21−47.
(21) Jeschke, G.; Matysik, J. *Chem. Phys.* **2003**, *294*, 239−255.
(22) Jeschke, G. *J. Am. Chem. Soc.* **1998**, *120*, 4425−4429.
(23) Polenova, T.; McDermott, A. E. *J. Phys. Chem. B* **1999**, *103*, 535−548.
(24) Feher, D.; Okamura, M. Y. In *The Photosynthetic Bacteria;* Clayton, R. K., Sistrom., W., Eds.; Plenum Press: New York, 1978; p 349−378.
(25) Okamura, M. Y.; Isaacson, R. A.; Feher, G. *Proc. Natl. Acad. Sci. U.S.A.* **1975**, *72*, 3491−3495.
(26) Fischer, M. R.; de Groot, H. J. M.; Raap, J.; Winkel, C.; Hoff, A. J.; Lugtenburg, J. *Biochemistry* **1992**, *31*, 11038−11049.
(27) Bennett, A. E.; Rienstra, C. M.; Auger, M.; Lakshmi, K. V.; Griffin, R. G. *J. Chem. Phys.* **1995**, *103*, 6951−6958.
(28) Hu, X. C.; Ritz, T.; Damjanovic, A.; Autenrieth, F.; Schulten, K. *Q. Rev. Biophys.* **2002**, *35*, 1−62.

Simulations. Numerical simulations of the photo-CIDNP effect were based on the theory described in ref 21 as implemented in a home-written Matlab program for density matrix computation using the EasySpin library.[29] The program starts from a pure singlet state of the pair and computes time evolution under a Hamiltonian including electron Zeeman, nuclear Zeeman, and hyperfine interaction as well as dipole–dipole and exchange coupling between the two electron spins. The part of the density matrix that decays to the ground-state from either singlet or triplet radical pairs is projected out (diamagnetic part) and is further evolved under a Hamiltonian including only the nuclear Zeeman interaction. Evolution is continued until radical pairs have completely decayed (100 ns) and after that nuclear polarization of the diamagnetic part of the density matrix is determined. As an extension to the approach described in ref 21, this procedure is performed for a full powder average, describing all interactions by tensors, except for the nuclear Zeeman interaction whose anisotropy is negligible on a time scale of 100 ns. A spherical grid (EasySpin function *sphgrid*) with 16 knots and C_i symmetry (481 orientations) was found to be sufficient for powder averaging. Nuclear polarization was normalized to the thermal polarization at the measurement temperature of 223 K.

As far as possible, parameters were taken from experimental work. Missing parameters were obtained by density functional theory (DFT) computations (see below). A lifetime of triplet radical pairs of 1 ns, a lifetime of singlet radical pairs of 20 ns, an exchange coupling $J = 7$ G, and a dipole–dipole coupling $d = 5$ G were assumed,[30–32] with a definition of the total electron–electron coupling Hamiltonian at an angle θ between the magnetic field axis and the vector connecting the paramagnetic centers in magnetic field units given by $-2J - d(3 \cos^2 \theta - 1)/2$.[21] The different lifetimes result from the different decay pathways of triplet pairs, which recombine to donor triplets, and singlet pairs, which recombine to the diamagnetic ground state. The principal values of the **g** tensor of the donor cation radical were taken as 2.00329, 2.00239, and 2.00203.[33] For the **g** tensor of the acceptor anion radical, we resorted to the values 2.00437, 2.00340, and 2.00239 for the bacteriopheophytin anion radical in *R. viridis*,[34] which we assume to be much closer to actual values for *Rb. sphaeroides* than values computed by DFT. Principal values of ^{13}C hyperfine tensors as well as all tensor principal axis systems were obtained by DFT.

DFT computations were performed with the program ADF 2004.1 using the BLYP functional.[35] The starting geometry was taken from the crystal structure of the photosynthetic reaction center of *Rb. sphaeroides* R26 in the charge-neutral state (PDB identifier 1AIJ).[36] The two chlorophyll molecules of the special pair as well as the two directly coordinated histidine residues (His L 173 and His M 202) were extracted for a donor model, and bacteriopheophytin C-6 was extracted for an acceptor model. Hydrogen atoms were added with the program Titan (Wavefunction, Inc., Irvine, CA). In this procedure some sp^3 carbons were wrongly assigned as sp^2 carbons; these were edited by hand to sp^3 in the same program. The phytyl chains in both the bacteriochlorophyll and bacteriopheophytin molecules were replaced by methyl groups, and the histidine residues were edited to methylimidazol ligands. A spin-restricted computation with the TZP basis set and frozen first shells for carbon and oxygen was used for geometry optimization of the acceptor anion radical and a spin-restricted

Table 1. Tentative Assignments of the ^{13}C Photo-CIDNP NMR Signals.

cofactor carbon no.	photo-CIDNP		cofactor carbon no.	photo-CIDNP	
	WT[a]	R26[b]		WT[a]	R26[b]
Φ13^1	189.4		Φ1, Φ3	138.3	138.8 E
L6	164.0	164.4 A	L4		136.8 A
M19	162.3	162.5 A	Φ2	134.0	133.7 E
M14	160.1	161.0 A	L12, M12		124.6 A
L9, M9	158.7	158.8 A	Φ12	119.4	119.7 E
M16	150.9	151.3 A	Φ15	108.5	106.8 E
L11	153.6	153.7 A	Φ10		101.3 E
M1		148.6 A	Φ5	97.4	97.8 E
L16	145.3	145.6 A	Φ20	94.9	95.2 E
M2	143.4	143.8 A			

[a] References 12, 13, and 39. [b] This work. A = absorptive, E = emissive.

computation with the DZ basis set and frozen first shells for carbon and oxygen for the special pair donor cation radical. Hyperfine couplings were computed in spin-unrestricted computations with a TZ2P all-electron basis set for the acceptor anion radical and a TZP all-electron basis set for the donor cation radical. Spin-restricted spin–orbit relativistic computations within the ZORA formalism[37] were used for **g** tensor computations, employing a TZ2P all-electron basis set for the acceptor anion radical and a DZP basis set for the donor cation radical. Control computations of EPR parameters in the starting geometries revealed only slight changes in the parameters that are smaller than the expected accuracy of the DFT computations (conservative estimates are ±20% for hyperfine couplings and ±5° for principal axes directions). For the donor cation radical, the computed principal axis directions could be compared to the experimental directions.[38] All three axes deviate by approximately 4° from the corresponding experimental axes, with the experimental errors being ±1 to 2°.

Chemical shift values for simulating photo-CIDNP spectra (Table 1) are taken from ref 13 with small changes as discussed in ref 39. For display, signals were represented by Gaussian peaks with a width of 0.5 ppm at all fields. This procedure is appropriate for comparison with experimental results as at higher fields, line broadening during signal processing was applied to improve signal-to-noise ratio.

Simulations of the coherent spin evolution in the radical pair state and DFT computations of hyperfine couplings for the triplet state of the special pair donor were performed as described in ref 13 for a single photocycle. Modifications of relative polarization during buildup under continuous illumination are neglected. The hyperfine anisotropy ΔA of individual carbon nuclei was calculated from the DFT-computed eigenvalues A_{xx}, A_{yy}, and A_{zz} of the hyperfine tensor as

$$\Delta A = A_{zz} - (A_{xx} + A_{yy})/2$$

where A_{zz} is the eigenvalue whose absolute value is maximum. Polarization originating from singlet and triplet pairs was stored separately. Nuclear spin relaxation in the triplet state was taken into account on the basis of the Solomon theory[40] by multiplying triplet polarization with a decay factor $\exp(-C\Delta A^2 T_T)$, where T_T is the lifetime of the special pair triplet. The parameter C takes the same value for all ^{13}C nuclei within the same spectrum but has to be fitted independently at different magnetic fields.

Results and Discussion

Polarization Pattern for the R26 Strain. The photo-CIDNP spectrum of R26 RCs (Figure 2A) exhibits peaks at very similar chemical shifts as the one of WT RCs (Figure 2B). However, signals at chemical shifts larger than 135 ppm are absorptive

(29) Stoll, S. Ph.D. Thesis, ETH, Zürich, 2003.
(30) Till, U.; Klenina, I. B.; Proskuryakov, I. I.; Hoff, A. J.; Hore, P. J. *J. Phys. Chem. B* **1997**, *101*, 10939–10948.
(31) Hulsebosch, R. J.; Borovykh, I. V.; Paschenko, S. V.; Gast, P.; Hoff, A. J. *J. Phys. Chem. B* **1999**, *103*, 6815–6823.
(32) Hulsebosch, R. J.; Borovykh, I. V.; Paschenko, S. V.; Gast, P.; Hoff, A. J. *J. Phys. Chem. B* **2001**, *105*, 10146–10146.
(33) Klette, R.; Torring, J. T.; Plato, M.; Möbius, K.; Bönigk, B.; Lubitz, W. *J. Phys. Chem.* **1993**, *97*, 2015–2020.
(34) Dorlet, P.; Rutherford, A. W.; Un, S. *Biochemistry* **2000**, *39*, 7826–7834.
(35) Velde, G. T.; Bickelhaupt, F. M.; Baerends, E. J.; Guerra, C. F.; van Gisbergen, S. J. A.; Snijders, J. G.; Ziegler, T. *J. Comput. Chem.* **2001**, *22*, 931–967.
(36) Stowell, M. H. B.; McPhillips, T. M.; Rees, D. C.; Soltis, S. M.; Abresch, E.; Feher, G. *Science* **1997**, *276*, 812–816.

(37) van Lenthe, E.; Wormer, P. E. S.; van der Avoird, A. *J. Chem. Phys.* **1997**, *107*, 2488–2498.
(38) Huber, M. *Photosynth. Res.* **1997**, *52*, 1–26.
(39) Prakash, S. Ph.D. Thesis, Leiden University, Leiden, 2006.
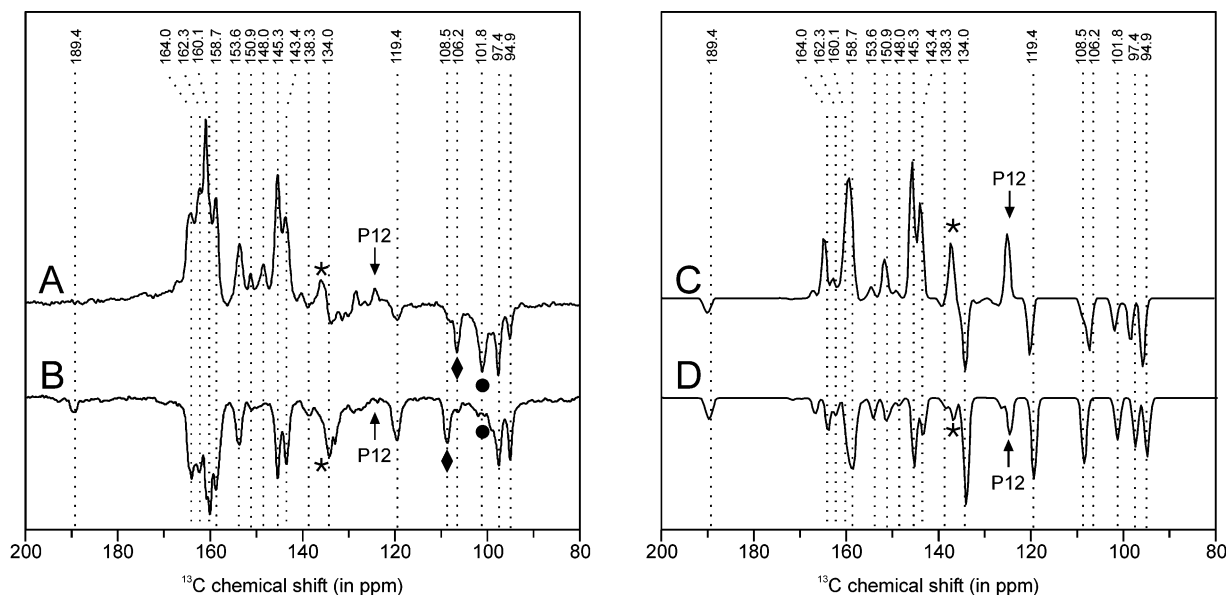(40) Solomon, I. *Phys. Rev.* **1955**, *99*, 559–565.

Figure 2. ^{13}C photo-CIDNP MAS NMR spectra of RCs of *Rb. sphaeroides*. Arrows, asterisks, diamonds, and full circles denote signals that appear to be sensitive to the environment of the RCs and are discussed in the text. Shown are experimental spectra of (A) R26 RCs and (B) WT RCs. The experiments have been conducted by 4.7 T. Simulated spectra shown are of (C) R26 RCs, assuming a lifetime of 100 μs for the triplet state of the special pair, and (D) WT RCs, assuming a lifetime of 100 ns for the triplet state of the pair.
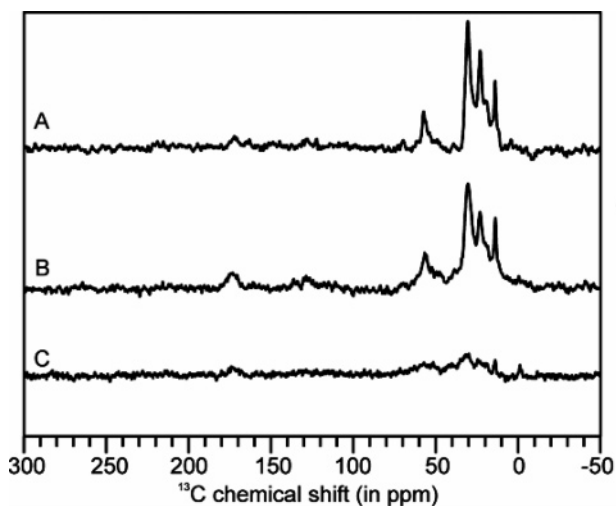
Figure 3. ^{13}C MAS NMR spectra of quinone depleted RCs of *Rb. sphaeroides* obtained at 223 K in dark at different magnetic field strengths of 17.6 T (A), 9.4 T (B), and 4.7 T (C).

Figure 4. ^{13}C photo-CIDNP MAS NMR spectra of quinone depleted RCs of *Rb. sphaeroides* obtained at 223 K in continuous illumination with white light at different magnetic field strengths of 17.6 T (A), 9.4 T (B), and 4.7 T (C).

for R26 in agreement with previous work,[7–10] whereas the whole spectrum is emissive for WT. The magnetic field dependence has been measured in dark (Figure 3) and in light (Figure 4) for RCs of R26 at (A) 17.6 T (750 MHz), (B) 9.4 T (400 MHz), and (C) 4.7 T (200 MHz). For RCs of WT, the field dependence has been measured in ref 13. This general photo-CIDNP pattern persists at all magnetic fields where the spectra were studied. Our previous assignment[13] suggests that the sign change is restricted to signals from ^{13}C nuclei of the special pair. Indeed, a simulation including the DR mechanism reproduces the sign change in this range of chemical shifts (Figure 2C,D) assuming $C = 4 \times 10^{-11}$ s and triplet lifetimes of 100 ns and 100 μs in WT and R26 RCs, respectively. We have tested the plausibility of the only fit parameter C by computing the longitudinal relaxation time T_1 for a hypothetic ^{13}C nucleus that is 5 Å away from a paramagnetic center with the same C value ($\Delta A = 159$ kHz). We find $T_1 = 0.99$ s. Given that the longitudinal relaxation
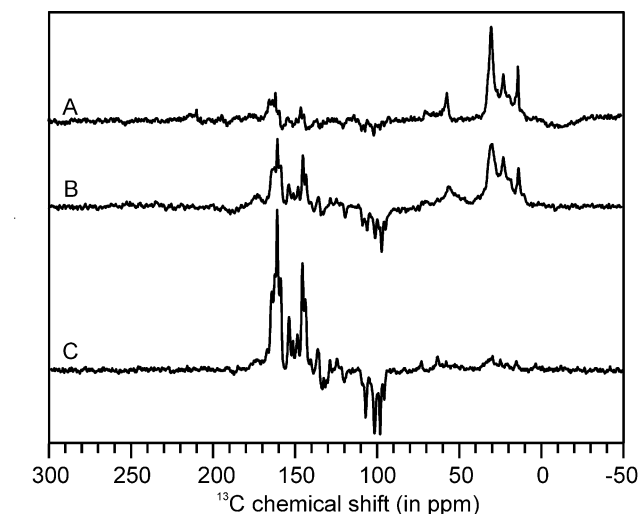
time of the ^{13}C nuclei in the diamagnetic ground-state is approximately 20 s, this appears reasonable, although we cannot make a quantitative assessment as we have no knowledge on rotational correlation times in the sample and we cannot assume that relaxation conforms to the Redfield limit. Note that the polarization pattern depends on the product of C with the triplet lifetime T_T. As C is a fit parameter, some deviation of T_T in our samples from the literature value cannot be excluded. The fast decay of polarization of some nuclei in the triplet state of the special pair is due to anisotropic hyperfine couplings of the order of 10 MHz. These large couplings are in turn caused by substantial spin density of up to 11.4% in p orbitals on these carbon atoms. The simulations also reproduce the field dependence of the polarization (Figure 5), with C values corresponding to $T_1 = 0.66$ s at 9.4 T and 0.40 s at 17.6 T for a hypothetical ^{13}C nucleus 5 Å away from the paramagnetic center.
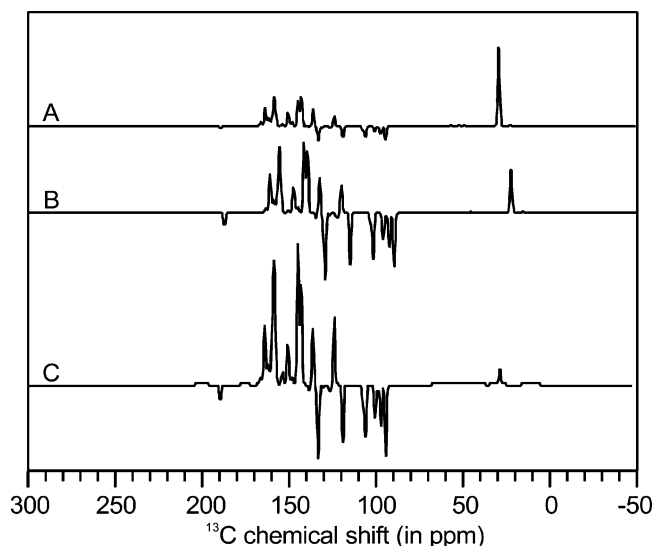
Figure 5. Simulated ^{13}C MAS NMR spectra RCs of *Rb. sphaeroides* strain R26 at different magnetic fields assuming a lifetime of 100 μs for the triplet state of the special pair. The magnetic fields are 17.6 T (A), 9.4 T (B), and 4.7 T (C).

In both, WT and R26 centers, the relative peak intensities are only broadly reproduced by the simulations (compare Figure 2 panels A and B with panels C and D). This is not unexpected, as experimental values like the exchange coupling between the two electron spins in the pair as well as lifetimes of singlet and triplet radical pairs and DFT-computed values, such as the ^{13}C hyperfine couplings, can well deviate by 20−30% from correct values. The only deviation that appears really significant is the substantial polarization of the ^{13}C nucleus C-L12/C-M12 that is predicted by the simulations for both WT and R26 centers, whereas only a weak emissive signal in R26 RCs is observed experimentally at 124.6 ppm (arrows in Figure 2).

Interestingly, earlier ENDOR[41] and special TRIPLE measurements[42] have detected a sizable isotropic proton hyperfine coupling for the methyl group attached to this carbon atom. This coupling changes strongly when His M202, which is directly coordinated to the special pair, is mutated to Leu or Glu. The unexpectedly low photo-CIDNP intensity at position C-L12/C-M12 may thus indicate an influence of the protein environment on the spin density distribution that is not accounted for in the simplified model of the RC used in our DFT computations.

Implications for Interpretation of Solid-State Photo-CIDNP Spectra. The broad agreement of the photo-CIDNP patterns and their field dependence between experiment and *ab initio* simulations for both WT and R26 RCs lends confidence to the notion that a combination of the DR, TSM, and DD mechanisms is responsible for the nonequilibrium nuclear polarization. Furthermore, the inversion of the sign of the donor signals supports our previous chemical shift assignments obtained in WT RCs[13] that were based on results from 2D NMR[12,39] and DFT computations of chemical shifts by others[43] and ourselves. Hence, signal assignment for R26 RCs is based on an experimental separation of donor and acceptor signals

(41) Lendzian, F.; Huber, M.; Isaacson, R. A.; Endeward, B.; Plato, M.; Bönigk, B.; Möbius, K.; Lubitz, W.; Feher, G. *Biochim. Biophys. Acta* **1993**, *1183*, 139−160.
(42) Lubitz, W.; Lendzian, F.; Bittl, R. *Acc. Chem. Res.* **2002**, *35*, 313−320.
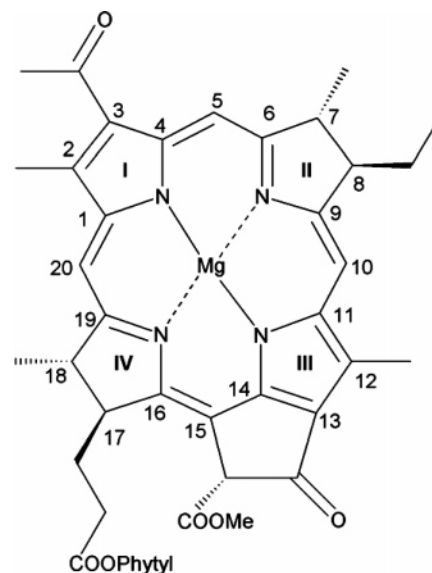(43) Facelli, J. C. *J. Phys. Chem. B* **1998**, *102*, 2111−2116.

Figure 6. Structure of bacteriochlorophyll *a* (BChl *a*) molecule with the numbering of carbon atoms using IUPAC nomenclature.

(Table 1, Figure 6) allowing for spectral editing controlled by different enhancement mechanisms. We may thus interpret the polarization pattern of WT RCs in terms of the spin density distribution in the radical pair state and the polarization change between the WT and R26 spectra in terms of the spin density distribution in the triplet state of the donor. To do so, we note that for all three mechanisms the polarization of a given ^{13}C nucleus is roughly proportional to the square of the anisotropic hyperfine coupling of that nucleus. The technique is thus particularly sensitive to spin density in p orbitals. For instance, the ^{13}C with a shift of 136.8 ppm (asterisks in Figure 2), assigned to C-L4 in the special pair, has a higher spin density in its p orbital in the triplet state than in the radical pair state, according to both experiment (Figure 2A,B) and simulation (Figure 2C,D).

The high sensitivity of chemical shifts to changes in the electronic structure of the ground-state allows for a detailed comparison of WT and R26 RCs. Two remarkable changes are apparent in Figure 2A,B. First, a strong peak is detected at 108.5 ppm in WT (♦) and a weak peak at 106.2 ppm, while in R26 the ratio is inverted. This peak is assigned to the acceptor nucleus C-Φ15.

Possibly, the difference may be due to different states of the protein pocket from which the quinone has been removed (see later). Second, the peak at 101.8 ppm that is predicted for both WT and R26 centers is actually observed only in R26 (●). This peak is assigned to acceptor nucleus C-Φ10, for which a strong signal has been calculated (Figure 2D). Therefore, the absence of this signal in Figure 2B indicates a disturbed environment, which may be due to the empty quinone pocket, while this pocket may be refilled with a substituting molecule maintaining the structure in Figure 2A.

Nanomolar Concentrations Probed in Intact Cells. The strong photo-CIDNP enhancement at a field strength of 4.7 T enables the study of cofactor molecules in their native cellular environment at a concentration of ∼100 nM without isotope enrichment. The dark spectrum of the intact cells of *Rb. sphaeroides* R26 (Figure 7A) shows broad peaks at 173 and 35 ppm. Under illumination (Figure 7B) the photo-CIDNP signals from the donor and acceptor appear.
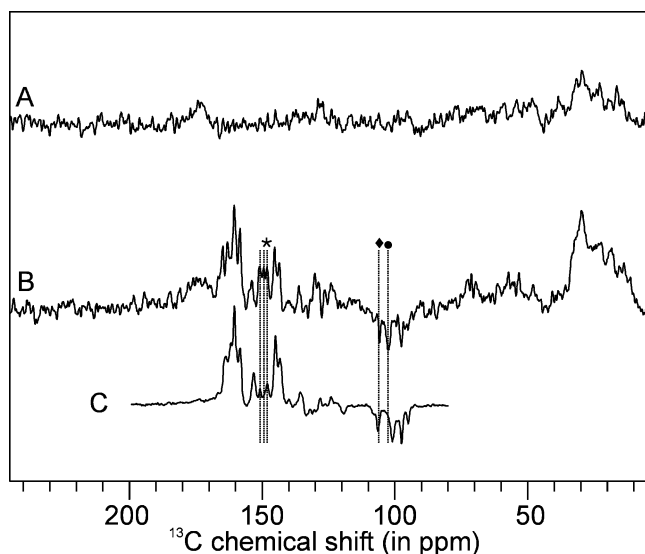
Figure 7. ^{13}C MAS NMR spectra of intact *Rb. sphaeroides* R26 cells at a field strength of 4.7 T and spinning frequency of 8 kHz in (A) dark and (B) light. The trace (C) shows a cutout from the spectrum of isolated RCs for comparison. Dotted vertical lines denote significant changes between cells and isolated RCs.

The light-induced signals appear in the region from 90 to 170 ppm. The overall photo-CIDNP intensity pattern is similar, but in some respects distinct from the spectrum of isolated reaction centres at 4.7 T (Figure 7C). The similarity between the photo-CIDNP spectrum from the isolated RCs and intact cells suggests that the ground-state electronic structure of the special pair is not strongly influenced by the surrounding protein complexes in the natural environment of an intact cell. The signals of acceptor nucleus C-Φ15 and C-Φ10 in R26 cells (♦, ●) (quinone-reduced) are observed at 106.1 and 102.3 ppm, in agreement with the isolated R26 RCs (quinone-depleted),

suggesting that in isolation the quinone binding site is not disturbed. This is in line with the conserved ratio of donor to acceptor signals for both samples, while previously an intensity change has been observed by ^{15}N photo-CIDNP MAS NMR.[8] In the shift range between 148 and 152 ppm (*), signals that we assign to C-M1 and C-M16 exhibit significantly stronger absorptive polarization in cells compared to isolated reaction centers. Considering the behavior of the same peaks in isolated RCs of WT and R26 as well as in cells, we can identify position C-M1 and C-M16 as a hot spot, where electron spin density appears to depend strongly on small changes in the environment of the special pair.

In conclusion, we have demonstrated that photo-CIDNP MAS NMR is a method to study selectively the electronic structure of photosynthetic cofactors at the molecular and atomic resolution as well as in an intact cell at natural abundance (1% ^{13}C). Combination with ^{13}C-isotope labeling is expected to further increase the signal by a factor of 100 to a total enhancement factor of a million. Such a strong polarization source might be used in the near future as a "spin torch" for illuminating the vicinity of RCs, or their artificial equivalents, by secondary polarization transfer.